Interactive Effects of Salinity, Redox State, Soil Type, and Colloidal Size Fractionation on Greenhouse Gas Production in Coastal Wetland Soils

N . D Ward[1-2*†], M. Bowe[1†], K. A. Muller[3], X. Chen[3], Q. Zhao[3], R. Chu[3], Z. Cheng[3], T. Wietsma[3], and R. K. Kukkadapu[3]

[1]Pacific Northwest National Laboratory, Sequim WA, 98382

[2]School of Oceanography, University of Washington, Seattle, WA 98105, USA

[3]Pacific Northwest National Laboratory, Richland, WA 99352, USA

*Corresponding author: Nicholas Ward (nicholas.ward@pnnl.gov)

†Contributed equally

Key Points:

- Sulfur and/or iron reduction limited anaerobic methane production in two of the three incubated freshwater and saline coastal soils
- Aerobic respiration was highest in soil with carbon composed of microbial detritus and a greater fraction of soluble vs. colloidal carbon
- Particulates and colloids comprised a major fraction of the saline soil's mobile carbon pool (58±9% and 19±7%, respectively)

Abstract

This study examines how greenhouse gas (GHG) production and organic matter (OM) transformations in coastal wetland soils vary with the availability of oxygen and other terminal electron acceptors. We also evaluated how OM and redox-sensitive species varied across different size fractions: particulates (0.45-1μm), fine colloids (0.1-0.45μm), and nano particulates plus truly soluble (<0.1μm; NP+S) during 21-day aerobic and anaerobic slurry incubations. Soils were collected from the center of a freshwater coastal wetland (FW-C) in Lake Erie, the upland-wetland edge of the same wetland (FW-E), and the center of a saline coastal wetland (SW-C) in Washington state. Anaerobic methane production for FW-E soils were 47 and 27,537 times greater than FW-C and SW-C soils, respectively. High particulate Fe^{2+} and dissolved sulfate concentrations in FW-C and SW-C soils suggest that iron and/or sulfate reduction inhibited methanogenesis. Aerobic CO_2 production was highest for both freshwater soils, which had a higher proportion of OM in the NP+S fraction (64±28% and 70±10% for FW-C and FW-E, respectively) and C:N ratios reflective of microbial detritus (1.7±0.2 and 1.4±0.3 for FW-E and FW-C, respectively) compared to SW-C, which had a higher fraction of particulate (58±9%) and fine colloidal (19±7%) OM and C:N ratios reflective of vegetation detritus (11.2 ± 0.5). The variability in GHG production and shifts in OM size fractionation and composition observed across freshwater and saline soils collected within individual and across different sites reinforce the high spatial variability in the processes controlling OM stability, mobility, and bioavailability in coastal wetland soils.

Plain Language Summary

Coastal wetlands, including freshwater systems near large lakes, rapidly bury carbon, but less is known about how they transport carbon either to marine/lake environments or to the atmosphere as greenhouse gases such as carbon dioxide and methane. Coastal wetlands face multiple threats that may alter how they cycle carbon such as sea level rise and lake level variability. We performed experiments on saline and freshwater coastal soils with and without oxygen present to understand what chemical factors drove greenhouse gas production. We also examined the different forms and size classes of carbon released from the soils when inundated and found that colloids, an understudied "solid" form of carbon smaller than particles but bigger than dissolved carbon, can represent anywhere from 1-44% of the total carbon released depending on soil type and oxygen availability. We also found that methane production in the absence of oxygen was nearly 28,000 times greater in a freshwater wetland soil compared to a saline soil that had competing reactions occurring such as iron and sulfur utilization. Carbon dioxide production in the presence of oxygen was greatest for samples with the highest proportion of carbon in the dissolved size fraction compared to larger colloids and particles.

1 Introduction

Vegetated coastal systems play a disproportionate role in carbon cycling compared to their land cover area, as they occupy only 0.07-0.22% of Earth's surface, yet account for approximately 10% of the net residual land C sequestration (Spivak et al. 2019). Accordingly, coastal wetlands are an area of significant interest in discussions of climate mitigation and solutions (Moomaw et al. 2018, Villa & Bernal 2018, Wang et al. 2019), though we currently lack a predictive

understanding of the complex and changing controls of carbon cycling in these dynamic systems (Ward et al. 2020). Increasing global temperatures are expected to alter wetland carbon storage via both enhanced productivity and decomposition (Kirwan & Blum 2011, Olsson et al. 2015), though this effect may be limited in colder environments (Sjögersten et al. 2014). In addition to the direct effects of rising temperatures, climate change and associated phenomena including relative sea level rise (SLR), lake level variability along large freshwater coastlines, and increasing occurrence and severity of extreme weather events like storm surge and hurricanes are predicted to increase the exposure of coastal systems to seawater and rainfall flooding (Tully et al. 2019, Wuebbles et al. 2019, Lønborg et al. 2020). These hydrological disturbances are expected to impact biogeochemical processing, with effects varying between wetlands of differing salinities, elevations, flooding frequency, and other antecedent conditions (Clark et al. 2007, Altor & Mitsch 2008, Noe et al. 2013, Stagg et al. 2017; Sengupta et al., 2021).

Soil as a dynamic organic matter (OM) pool is a crucial component of the global carbon cycle (Stockmann et al. 2013, Rodrigo-Comino et al. 2020, Lal et al. 2021). Likewise, the quantity and quality of carbon exported laterally from coastal wetlands is poorly quantified and may serve as an important, but under examined carbon sink (Santos et al. 2021). Soil OM in the aqueous phase can transition between particulate, colloidal, and dissolved forms in soil and may be stabilized or transported out of soil—a fate that is influenced by a complex mixture of factors (Marín-Spiotta et al. 2014). Anoxic conditions have been shown to promote dissolved organic carbon (DOC) release from soil in nitrate-reducing conditions, but markedly decrease DOC release under sulfate-reducing and methanogenic conditions (Kim & Pfaender 2005). Other work has found increased DOC release under reducing conditions due to associated pH increases and reduction of reactive iron and manganese (Grybos et al. 2009). Increased salinity is also thought to induce flocculation of OM, particularly humic substances, and inhibit extraction of OM from soils (Kida et al. 2017). The complexities of how soil OM fractionates across different size fractions, and the relative reactivity of these fractions, is not currently considered in our understanding of lateral carbon export from coastal wetlands (Maher et al. 2013, Ho et al. 2017, Chu et al. 2018)

In addition to export out of wetland soils, OM can be decomposed in soil and yield greenhouse gas (GHG) release, the rate of which is also influenced by a combination of environmental, geochemical, mineralogical, and microbial factors (Schmidt et al., 2011; Patel et al., 2022). Reducing conditions lower decomposition rates via a hypothesized mechanism referred to as the "enzymic latch," in which anoxia inhibits the activity of phenol oxidase enzymes (Freeman et al. 2001). More recently Wang et al. (2017) have implicated iron oxidation in regulating phenol oxidation activity in oxic conditions and counteracting the "latching" effect of oxygen to phenol oxidases. Though in oxic soils iron (hydr)oxides contribute to OM storage (Wagai & Mayer 2007), in anoxic conditions iron hydroxides acting as terminal electron acceptors can increase OM decomposition (Buettner et al. 2014, Chen et al. 2020). Observed effects of increasing salinity on soil decomposition rates have varied across field and lab studies, and include stimulation of decomposition (Stagg et al. 2018), inhibition (Neubauer et al. 2013, Qu et al. 2019, Zhang et al. 2022), stimulation of CH_4 release with inhibition of CO_2 (Zhang et al. 2022), negligible methane emissions in polyhaline marshes (Poffenbarger et al. 2011), and a quadratic relationship with initial decrease in decomposition with increasing salinity followed by heightened decomposition at higher salinities (Stagg et al. 2017). One proposed mechanism contributing to altered GHG emissions with salinity is that the sulfate found in seawater has been associated with increased sulfate reduction rates (Weston et al. 2011) and thus increased CO_2

emissions from carbon mineralization (Feng & Hsieh 1998), though not consistently across studies (Herbert et al. 2015). Sulfate exposure in wetland soils has also been observed to suppress methanogenesis (Helton et al. 2019).

The heterogeneous nature of soil environments complicates the interpretation of the biogeochemical behaviors described above. Biogeochemical processes can be highly influenced by heterogenous characteristics such as soil microsites (Parkin et al., 1987) and differing pore sizes (Bailey et al., 2017) among other factors. The size distribution of water-soluble OM and redox-sensitive elements in soil porewaters is one such factor that might play a key role in determining the mobility and/or reactivity of OM in soils. Laboratory characterizations of OM often focus on DOC, operationally defined as the carbon that passes through filters ranging in pore size from 0.2 to 0.7 μm; this practice has been recently questioned due to the resulting overestimation of truly soluble DOC via the inclusion of colloids (Yan et al. 2018, Afsar et al. 2020, 2023). The importance of understanding the role of colloids in soil carbon cycling stems in part from their highly reactive surfaces that permit binding to OM (Rod et al. 2020). Thus, understanding how the biogeochemical behavior of colloidal size fractions varies under different environmental and mineralogical conditions is central to constraining the mechanisms underlying soil OM transport and transformation.

Coastal wetland salinity exposure and redox conditions are predicted to change in response to altered precipitation patterns, SLR, and storm surge, making an understanding of the compounding effects of these disturbances on wetland soil OM transport, decomposition, and storage particularly important (Spivak et al. 2019, Moomaw et al. 2018). Given the array of factors influencing carbon cycling changes in coastal wetlands in response to redox shifts and inundation, we sought to examine how GHG production and OM transformations in soils collected from different freshwater and saline wetland settings varied under aerobic versus anaerobic conditions and in the presence of other terminal electron acceptors.

During 21-day incubations conducted in aerobic and anaerobic conditions, we tested how oxygen availability, soil origin, and inundation history influence the evolution of GHG production, bulk chemical properties, redox sensitive species, and biodegradation of OM across three size fractions: nano particulates plus truly soluble OM (NP+S; < 0.1 μm), fine colloids (FC; 0.1-0.45 μm), and particulates (P; 0.45-1 μm). We hypothesized that anaerobic methane production would be outcompeted by iron or sulfate reduction for soils with exposure to high levels of either aqueous or mineral-derived sulfate and iron, and that the relative proportion of soluble versus mineral-associated colloidal and particulate OM would be an important factor mediating aerobic respiration.

2 Materials and Methods

2.1 Soil Collection

Two surface soil samples were collected from a freshwater site (FW), located near the outlet of Old Woman Creek into Lake Erie (Huron, Ohio, United States). These samples were collected at the wetland center (i.e., in the center of the wetland, FW-C; 41.37613787°, -82.50754702°) and at the upland-wetland edge (i.e., near the border between where wetland vegetation starts transitioning to upland vegetation, FW-E; 41.37590722, -82.5071329°). FW-C soils are

characterized primarily as frequently flooded silty fluvaquents; FW-E soils are occasionally flooded and characterized primarily as Holly silt loam (USDA Natural Resources Conservation Service n.d.). In general, the freshwater site is characterized by surface water with salinity generally between 0.1 and 0.3 PSU, and dissolved oxygen (DO) ranging from 5-15 mg/L (NOAA NERRS 2022). At the time of soil collection on 12/9/2021, porewater DO was 10.5 mg/L at FW-E and 1.5 mg/L at the FW-C, measured using a YSI Pro Plus multiparameter sonde connected to a porewater sipper rod (M.H.E. products).

A third sample was collected at the center of a saline wetland (SW-C) from the floodplain of Beaver Creek (46.905938°, -123.978047°), a tidally influenced first-order tributary draining into Johns River, which flows into the Grays Harbor estuary in Washington state. Beaver Creek floodplain soils are characterized as hydric Ocosta silty clay loam (USDA Natural Resources Conservation Service n.d.) and soil texture is primarily silty clay, but ranges from sandy clay loam to clay (Sengupta et al., 2019). Groundwater in this floodplain is generally anaerobic and has salinities between 15-30 PSU during dry periods and 5-20 PSU during wet periods (Regier et al. 2021). Detailed site information is described by Yabusaki et al. (2020). When the soil was collected on 1/25/2022, porewater DO was 2.2 mg/L and salinity was 3.6 PSU. All soil samples were collected at approximately 30 cm depth and were stored in sealed bags at 4°C prior to incubation.

2.2 Incubations and Greenhouse Gas Analyses

Prior to soil incubations, the soils were conditioned in a Coy anaerobic chamber at O_2 levels below 20 ppm for four days. Vegetation and rocks were removed by hand. A subsample of each soil was dried in aerobic conditions for bulk characterization [total C (TC), total nitrogen (TN), and total sulfur (TS)]. Field moist soil was suspended in deoxygenated de-ionized water in 1 L microcosms with ~250 mL headspace and shaken for 5 minutes, the end of which marked the initial timepoint (referred to as “pre-incubation”). Soil:water weight ratios were determined by drying subsamples of soils to find percent moisture and were 1:12.7 for FW-C soil, 1:16.5 for FW-E soil, and 1:11.0 for SW-C soil.

At the initial timepoint, triplicate bottles were destructively sampled for chemical analyses. A subset of bottles were incubated under anaerobic incubations; bottles were shaken within the anaerobic chamber with deoxygenated water, and headspaces were purged with N_2 gas five days per week following GHG sampling. Aerobic incubations were initiated by adding water with ambient O_2 levels. Bottles were shaken with ambient air and the suspension was allowed to equilibrate with ambient air beforehand, and headspaces were purged with room air throughout the incubations. After shaking, headspaces were sampled with 60 mL syringes via lids fitted with two luer valves for gas analysis, which were then sealed. Incubations were carried out in the dark for 21 days at temperatures between 19-21°C before destructive sampling of soil and the supernatant for a variety of size-fractionated analyses.

Headspace gas was sampled 5 days per week (i.e., Monday through Friday) during incubations, at which point incubations were shaken vigorously for 60 seconds to homogenize and equilibrate aqueous incubate with headspace. Oxygen content was measured with an optical oxygen meter to confirm the extent of anoxic conditions or anoxia (Pyroscience, FireSting GO_2). Partial pressures

of headspace CO_2 and CH_4 were measured via a cavity ring-down spectrometer (Picarro, G2508 Gas Concentration Analyzer).

2.3 Size-fractionated Chemical Analyses

At the start and end of incubations, liquid suspensions were divided into 50-mL centrifuge tubes and centrifuged to generate supernatants of three size fractions:

(1) <1 μm [a mixture of soluble OM (S; <10 kDa - 2.5 nm), mineral-associated nanoparticulate colloids (NP; 2.5 nm - 0.1 μm), mineral-associated fine colloids (FC; 0.1 μm-0.45 μm), and mineral-associated particulate organic matter (P; 0.45 μm - 1.0 μm)];

(2) <0.45 μm [a composite of soluble OM, nanoparticulate, and fine colloidal fractions (although each of these fractions are present in < 0.45 μm filtered samples, this fraction is often erroneously referred to as soluble dissolved organic carbon)] and;

(3) <0.1 μm (nanoparticulate and soluble OM), following the methods of Afsar et al. (2020). Pre-incubation samples and anaerobic incubations were handled in an anaerobic chamber to maintain anoxia prior to analyses.

Size-fractionated and bulk (i.e., unfiltered) pre-incubation and incubated samples were analyzed on an automatic titrator (Mettler-Toledo, T7 Excellence) for pH, alkalinity, and oxidation-reduction potential (ORP; Figures S1-2). Size-fractionated slurry samples were also analyzed for ferrous iron (Fe^{2+}) concentration by colorimetric assay (Thermo Scientific, FerroZine™ iron reagent) and total iron content and abundance via ICP-OES (Perkin Elmer, Optima 7300 DV). Ferrous iron concentration was analyzed using the ferrozine assay (Stookey, 1970). Briefly, 0.4 mL of well-mixed sample was added to 4 mL of 1 g/L ferrozine in 20 mM PIPES (piperazine-1,4-bis (2-ethanesulfonic acid)) buffer at pH 7 and shaken to homogenize. After five minutes, the solution was measured for the absorbance at 562 nm by an ultraviolet–visible spectrophotometer (UV–Vis) (Evolution 260 BIO, Thermo Scientific).

Sulfate and nitrate concentrations were measured via ion chromatography (ThermoFisher, Dionex ICS-6000 HPIC). Due to instrument limitations, it was not possible to analyze by size fractions without damaging the instrument, so samples were filtered to 0.2 μm prior to analysis.

Aqueous TOC and TN concentrations were measured on size-fractionated and bulk samples on a Shimadzu TOC-L. Samples were stirred via a magnetic stir bar during analysis to ensure homogeneity.

At the start and end time points of incubations, solid soils remaining in the bottom of reactors were subsampled, and soils from triplicates within treatments were homogenized together prior to oven drying. The combined dry soil sample was analyzed for TC, TN, and TS (Elementar vario EL Elemental Analyzer; Figures S3-5).

Supernatant samples were characterized by 21T Fourier transform ion cyclotron resonance mass spectrometer (FTICR-MS) located at the Environmental Molecular Sciences Laboratory (Richland, WA). Samples were randomized and directly infused into the FTICR-MS, after SPE clean-up (Dittmar et al. 2008), via an automated direct infusion cart (Orton et al. 2018). Samples

were measured in negative electrospray ionization (-ESI) polarity with technical replicates. All spectra were peak picked, internally calibrated and chemical formulae assigned using Formularity (Tolić et al. 2017) considering only the presence of C, H, O, N, S and P.

2.4 Data Analysis

The concentration of CO_2 and CH_4 in the headspace and dissolved in incubates were calculated using Henry's law, the ideal gas law, and temperature-dependent coefficients from Weiss (1974), Wiesenburg & Guinasso (1979), and Weiss & Price (1980). See Magen et al. (2014) for relevant equations. Cumulative moles of each gas produced during incubations were determined by correcting for gas removed during sampling and added during headspace purging. The room air used to purge the aerobic incubations after each gas sampling was measured with the cavity ring-down spectrometer (Picarro, G2508 Gas Concentration Analyzer) so that the amount of CO_2 and CH_4 added to the headspace was known.

Chemical concentrations in each individual colloidal size fraction (e.g., <0.1 µm, 0.1-0.45, and 0.45-1 µm) were calculated by subtraction. TOC, TN, and Fe^{2+} concentrations in the largest size fraction (0.45-1 µm, or OM solely associated with particulates referred to as "P" throughout) were deduced by subtracting data from the <0.45 µm samples. Size-fractionated values for the medium-size fractions (0.1-0.45 µm, or solely fine colloids, referred to as "FC" throughout) were determined by subtracting values from the <0.1 µm (smallest size; composite of nanoparticulates and truly soluble OM, referred to as "NP+S" throughout) samples from those of the <0.45 µm samples. C:N ratios were calculated for aqueous samples using TOC and TN values and were calculated for solid soils using TC and TN data.

All statistical analyses were performed in the statistical computing language R using R Studio version 2023.09.0+463 (RStudio Team, 2020). Paired t-tests, using Benjamini & Hochberg p value adjustment were used to compare significant differences in chemical concentrations between pre- and post-incubation samples, incubation types, soil types, and size fractions. Reported p values represent comparisons of one group to another. Significant differences were considered to fall within a 95% confidence interval (i.e., $p < 0.05$). Pearson correlation was used to compare linearity in GHG production rates across the different experiments.

3 Results

3.1 Greenhouse Gas Production

First, we describe how GHG production varied across the different soil types and incubation conditions. After 21 days under aerobic conditions, the FW-C and SW-C soils produced similar amounts of CO_2 (9.17 ± 0.82 and 7.72 ± 0.41 mmol C / kg dry soil by the end of the experiment, respectively; $p > 0.05$), whereas the FW-E soils produced significantly more CO_2 by day 21 of the incubation (13.8 ± 2.14 mmol C / kg dry soil; $p < 0.05$). In addition to the FW-E soils producing more CO_2 under aerobic conditions, the rate of CO_2 production peaked after seven days (Figure 1), resulting in a less linear behavior over the course of the 21-day incubation ($R^2 = 0.72$) compared to FW-C ($R^2 = 0.94$) and SW-C soils ($R^2 = 0.98$).

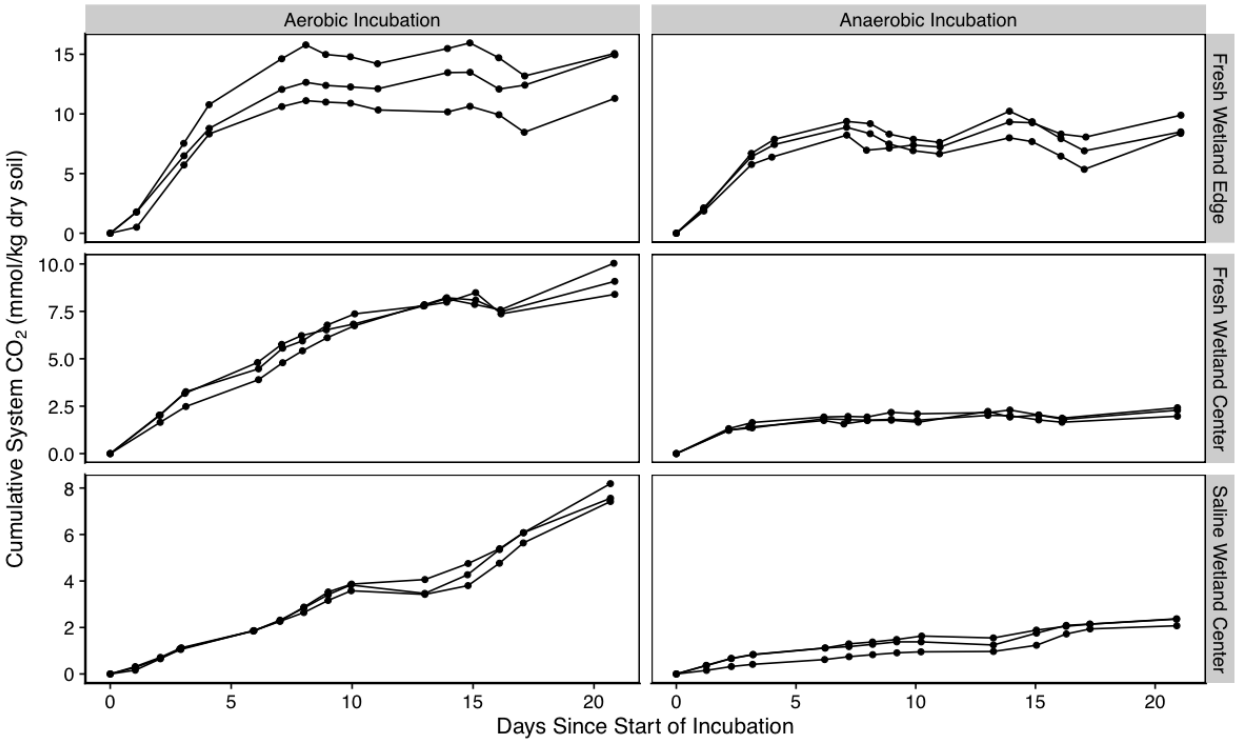

Figure 1. Net carbon dioxide production during incubations expressed per kg of dry soil. Note that y-axis scaling varies between top, middle, and bottom panels to allow trends to be seen more clearly.

For all three types of soils, total CO_2 production over the 21-day experiment was lower under anaerobic conditions compared to the same soil incubated under aerobic conditions. Aerobic CO_2 production was 4.1, 1.5, and 3.4 times greater than anaerobic production for FW-C, FW-E, and SW-C soils, respectively ($p < 0.05$). Likewise, when considering all soil types together, the aerobic experiments produced 2.3 times more CO_2 than the anaerobic experiments at the end of the experiment ($p < 0.05$). As with the aerobic experiments, after 21 days under anaerobic conditions, the FW-C and SW-C soils produced similar amounts of CO_2 (2.22 ± 0.23 and 2.27 ± 0.17 mmol C / kg dry soil, respectively; $p > 0.05$), whereas the FW-E soils produced significantly more CO_2 (8.92 ± 0.85 mmol C / kg dry soil; $p < 0.05$). The temporal behavior of CO_2 production observed in the anaerobic experiments (Figure 1) were similar to the aerobic experiments with FW-E peaking around day 4 and exhibiting the least linear behavior ($R^2 = 0.66$) compared to FW-C ($R^2 = 0.73$) and SW-C ($R^2 = 0.93$).

A small, but negligible amount of CH_4 production was detected for all three soil types under aerobic conditions (Figure 2). After 21 days under aerobic conditions, SW-C soils produced the least CH_4 (0.390 ± 0.061 µmol C / kg dry soil), followed by FW-C (4.16 ± 3.56 µmol C / kg dry soil), and FW-E (49.7 ± 47.0 µmol C / kg dry soil). Similar to CO_2 production, the difference in aerobic methane production was significant between FW-E and the other two soil types ($p < 0.05$), whereas FW-C and SW-C were not significantly different ($p > 0.05$).

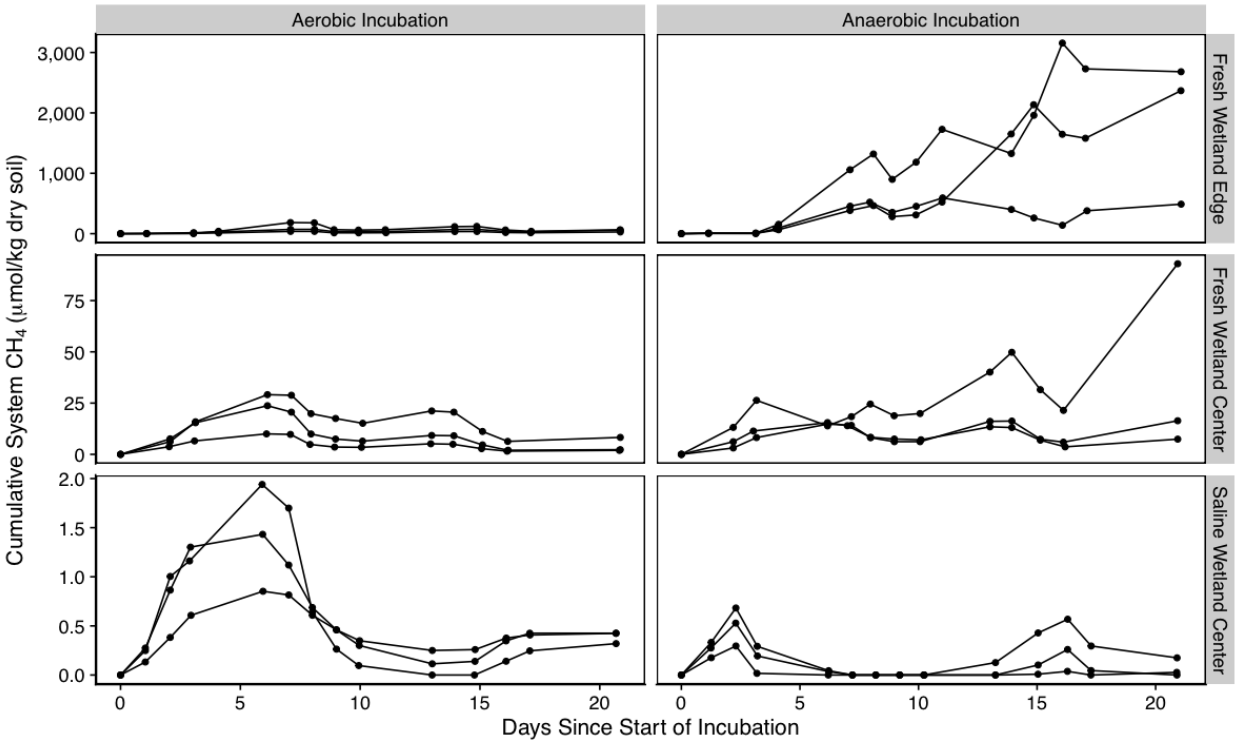

Figure 2. Net methane production during incubations expressed per kg of dry soil. Note that y-axis scaling varies between top, middle, and bottom panels to allow trends to be seen more clearly.

The minimal methane production under aerobic conditions was to be expected; however, interestingly, even under anaerobic conditions CH_4 production was low for FW-C and SW-C soils (38.9 ± 47.0 and 0.067 ± 0.094 µmol C / kg dry soil by the end of the incubation, respectively), suggesting that other redox processes inhibited methanogenesis during the incubations (Figure 2). In contrast, FW-E soils had substantially higher amounts of CH_4 ($p < 0.05$) produced after 21 days (1,845 ± 1,186 µmol C / kg dry soil) with methane production not initiating until day four. It is possible that methane production may have occurred in the FW-C and SW-C soils if incubated longer, allowing other terminal electron acceptors to be exhausted.

The molar ratio of CO_2:CH_4 varied substantially between incubation conditions, ranging from a minimum value of 2.51 in the FW-E anaerobic experiment to a maximum value of 225,206 in the SW-C anaerobic experiment (Figure S6). The average CO_2:CH_4 ratio for the final time point (day 21) of the anaerobic experiments was lowest for FW-E (8.98 ± 9.76), followed by FW-C (152 ± 144) and SW-C (49,295 ± 52,940); despite the large differences in mean ratios at the end of the experiment, differences between soil types were not significant given the large variability between triplicates ($p > 0.05$). The average CO_2:CH_4 ratio for the final time point (day 21) of the aerobic experiments was similarly lowest in the FW-E soils (299 ± 89.5), followed by FW-C (3,386 ± 2,134) and SW-C (20,121 ± 3,186); in this case there was a significant difference between SW-C and FW-E ($p < 0.05$).

3.2 Physiochemical Conditions of the Incubations

To contextualize the physiochemical conditions each soil experienced during the incubations, we first examine changes in ORP, pH, and alkalinity. ORP of all size ranges of both freshwater wetland soils increased after being incubated under aerobic conditions for 21 days (Figure S1). In contrast, ORP decreased, albeit to a smaller degree, in the saline samples under both aerobic and anaerobic conditions (Figure S1). The observed increase in ORP for freshwater samples incubated under aerobic conditions was significant ($p < 0.05$) for all size fractions except for the bulk size fraction for FW-E, the <1 μm size fraction for FW-C soils, and the <0.45 μm size fraction for FW-E soils ($p > 0.05$). The decrease in ORP under aerobic conditions observed for SW-C was significant ($p > 0.05$) for all size fractions except for the bulk unfiltered sample ($p > 0.05$). Under anaerobic conditions, ORP decreased for all the size ranges in FW-C and SW-C incubates but was marginally higher for the FW-E soils. These differences were statistically significant except for the <1 μm size fraction for FW-C soils, <0.45 μm size fraction for FW-E soils, and <0.1 μm size fraction for FW-C soils. ORP reached negative values in all but the smallest size fraction (<0.1 μm) for SW-C soils.

Alkalinity of the incubated solutions was measured to understand differences in cation and carbonate/bicarbonate exchange between the soil matrix and each size fraction. Alkalinity increased in all three soil types after being incubated under anaerobic conditions ($p < 0.05$). Alkalinity also increased in all soils and size fractions under aerobic conditions, but to a smaller extent (Figure S1); these changes were statistically significant in all cases except for the bulk and <0.1 μm size fraction for FW-E soils ($p < 0.05$). pH was generally higher in the anaerobic incubations compared to aerobic and ranged from 6.0 to 7.7 across all size fractions, soil types, and incubation conditions (Figure S2).

3.3 Competing Redox Reactions

Next, we examine how a variety of redox-sensitive elements evolved throughout the incubations, possibly influencing the observed trends in GHG production particularly in the anaerobic incubations where O_2 was not available as a terminal electron acceptor. We also assess how each parameter is speciated across different size fractions (when analytically feasible) to understand the dominant forms found across the studied soil types and redox states.

First, we evaluate nitrate as a potential competing terminal electron acceptor (Figure 3). The highest pre-incubation dissolved (<0.2 μm) nitrate concentrations were observed in the FW-E soils (2.26 ± 0.76 mg/L) compared to FW-C (0.48 ± 0.24 mg/L) and SW-C soils (0.01 ± 0.02 mg/L). Nitrate levels decreased significantly ($p < 0.05$) under both aerobic and anaerobic conditions for the FW-E soils (Figure 3). While there was slight variability in nitrate levels in the incubated FW-C and SW-C soils, none of these changes were significant ($p > 0.05$). All three soils had barely detectable nitrate levels under anaerobic conditions (0.06 – 0.19 mg/L) suggesting that nitrate reduction likely did not prevent methanogenesis from occurring during the 21-day incubation.

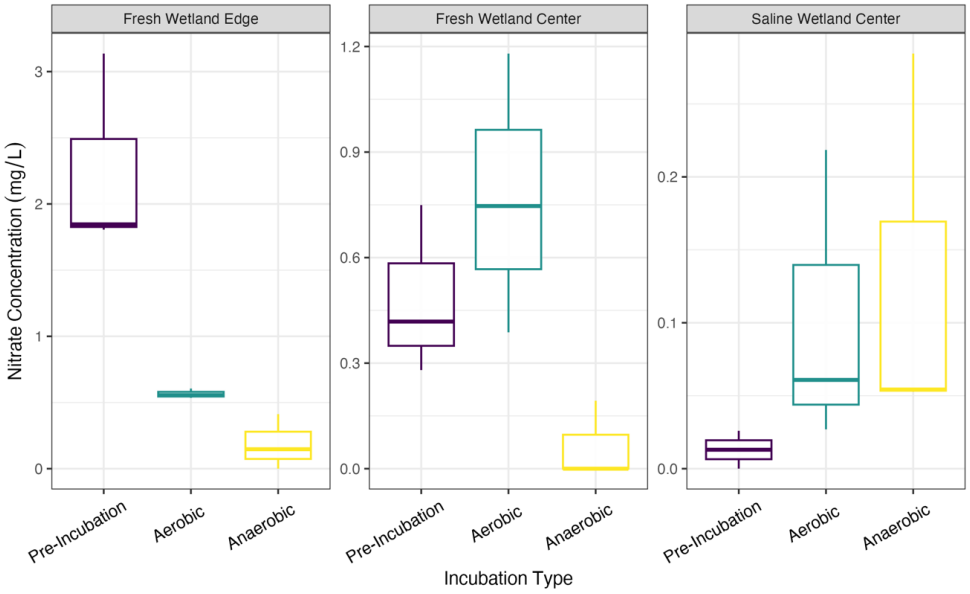

Figure 3. Nitrate concentrations in samples filtered to 0.2 μm pre- and post-incubation. The instrumentation used to measure nitrate did not allow us to analyze by colloidal size fraction without compromising the instrument.

Iron species were measured to assess how much total iron was present initially and how much reduced iron (Fe^{2+}) was present in the aqueous phase to assess if iron reduction potentially competed with methanogenesis in any of the soil samples. Total iron at the beginning of the incubation was two orders of magnitude higher for SW-C soils compared to both freshwater soils (Figure 4; $p < 0.05$). For both freshwater soils, most of the iron was present as particulates and fine colloids with minimal nanoparticulate and soluble iron present (Figure 4). Fine colloids were the largest source of total iron for the SW-C soils and in contrast to the freshwater soils there was appreciable amounts of nanoparticulate and soluble iron prior to the incubations.

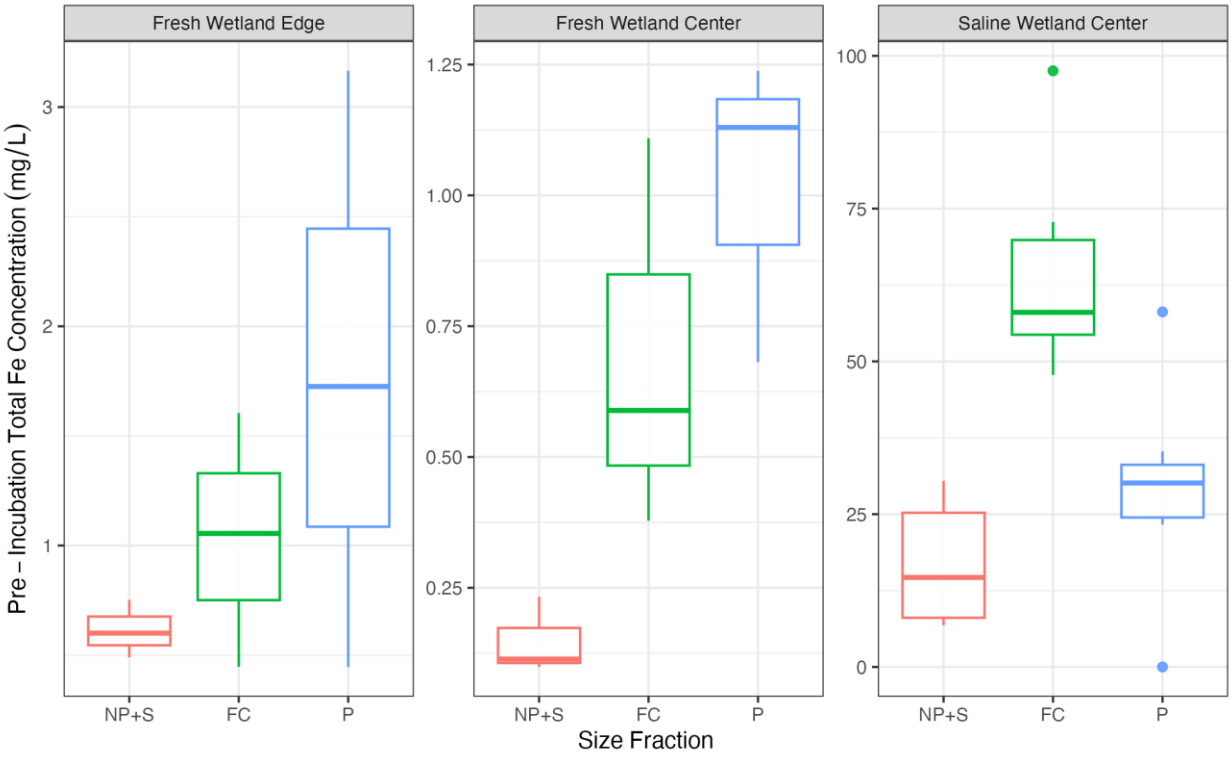

Figure 4. Concentrations of total iron across size fractions prior to incubation. It was not possible to analyze post-incubation samples due to logistical constraints.

Similar to total iron, there was minimal Fe^{2+} present in both freshwater samples prior to the incubation (Figure 5). Adding up all three size fractions (i.e., Fe^{2+} present in all forms < 1µm), the average initial Fe^{2+} concentration was 0.38 ± 0.25 µg/L for FW-E and 0.20 ± 0.17 µg/L for FW-C compared to an initial concentration of 18.4 ± 15.7 µg/L for SW-C. Particulates (i.e., 0.45-1.0 µm) were the dominant form of Fe^{2+} found in the pre-incubation samples for SW-C soils (73 ± 19% of the Fe^{2+} pool), whereas particulates and fine colloids contributed roughly equally for the FW-E soils, and Fe^{2+} was mostly present in the smallest NP+S fraction (67 ± 48%) for the pre-incubation FW-C soils (Figure 5).

For the FW-E soils, there was a slight increase in Fe^{2+} concentrations (all fractions, < 1µm) after incubating under anaerobic and a slight decrease under aerobic conditions (Figure 5), but these changes were not significant ($p > 0.05$). When considering each size fraction independently, there was a significant increase in the NP+S fraction under anaerobic conditions and decrease under aerobic conditions ($p < 0.05$), whereas there were no significant changes in the FC or P fractions. Collectively, these results indicate that iron reduction likely did not outcompete methanogenesis during the FW-E incubations.

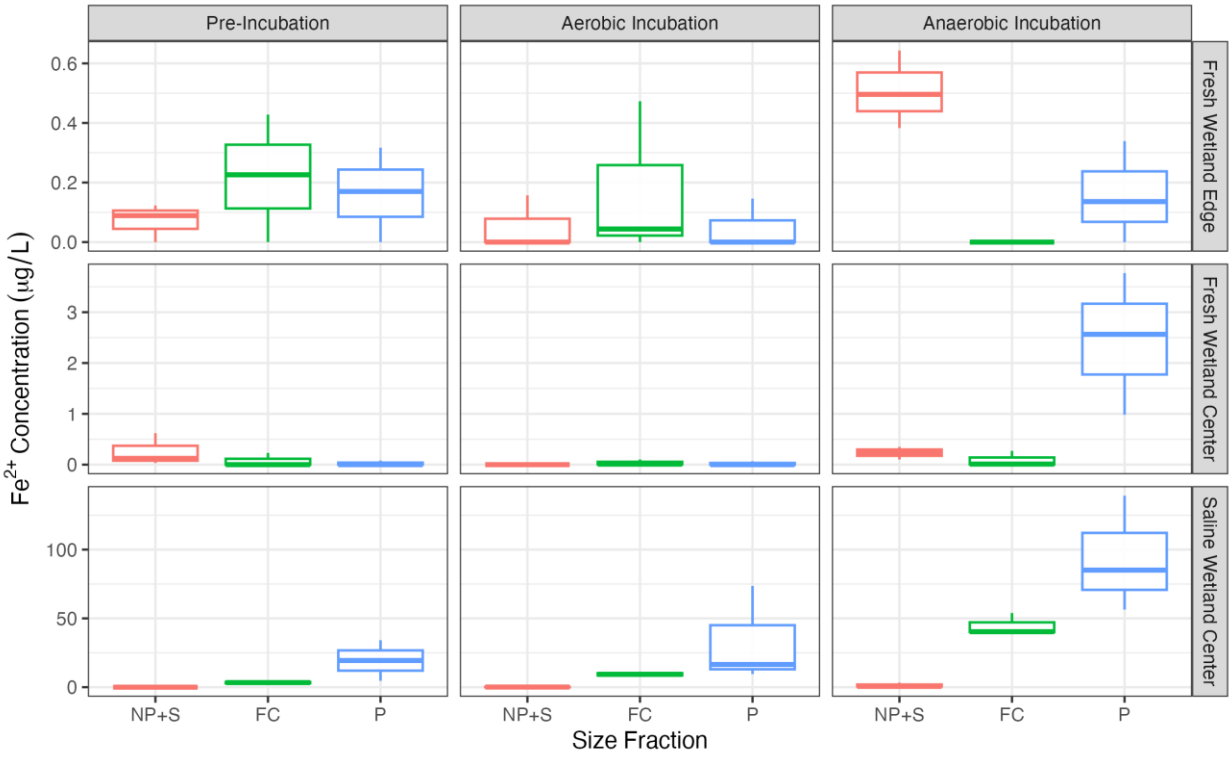

Figure 5. Concentrations of Fe^{2+} across size fractions and incubation conditions. The smallest size fraction is nanoparticulates plus truly soluble material (NP+S; <0.1µm), followed by fine colloids (FC; 0.1-0.45µm), then particulates (P; 0.45-1µm).

For the FW-C soils, Fe^{2+} concentrations (all fractions, < 1µm) similarly decreased under aerobic conditions, but the change was not significant ($p > 0.05$). In contrast to FW-E, Fe^{2+} concentrations increased significantly to 2.70 ± 1.11 µg/L (all fractions, < 1µm) under anaerobic conditions for the FW-C soils ($p < 0.05$). In the case of FW-C soils, there was a shift in the size distribution of Fe^{2+}, with 84 ± 19% of the Fe^{2+} present under anaerobic conditions found in the particulate size fraction. These results suggest that iron reduction may have inhibited methane production to some extent during the 21-day incubation for FW-C soils.

SW-C, the soils with the lowest methane accumulation, had the highest Fe^{2+} levels initially and under both incubation conditions. In contrast to the other experiments, Fe^{2+} concentrations (all fractions, < 1µm) increased under both aerobic (42.6 ± 36.6 µg/L) and anaerobic conditions (140 ± 43 µg/L; $p < 0.05$; Figure 5). The majority of Fe^{2+} was present as particulates under both aerobic (69 ± 16% of the Fe^{2+} pool) and anaerobic (65 ± 10%) conditions. The fine colloid fraction contained most of the remaining Fe^{2+} with less than 1% of the Fe^{2+} present in the smallest NP+S fraction. These results suggest that iron reduction was likely an important process that limited methanogenesis for the SW-C soils.

Continuing down the redox ladder, dissolved (<0.2 µm) sulfate concentrations were measured to determine whether sulfate reduction may have been a factor that inhibited methanogenesis in our experiments. Average initial aqueous sulfate concentrations from the SW-C soil (129 ± 1 mg/L) were substantially higher than for the FW-E and FW-C soils (3.38 ± 0.36 mg/L and 17.6 ± 1.9

mg/L, respectively; $p < 0.05$; Figure 6). During the incubations, there was a strong scent of hydrogen sulfide detected while purging the headspace of the SW-C soils held under anaerobic conditions, suggesting active sulfate reduction was occurring. Although H_2S was not directly measured, we did not smell H_2S in the other soil incubations.

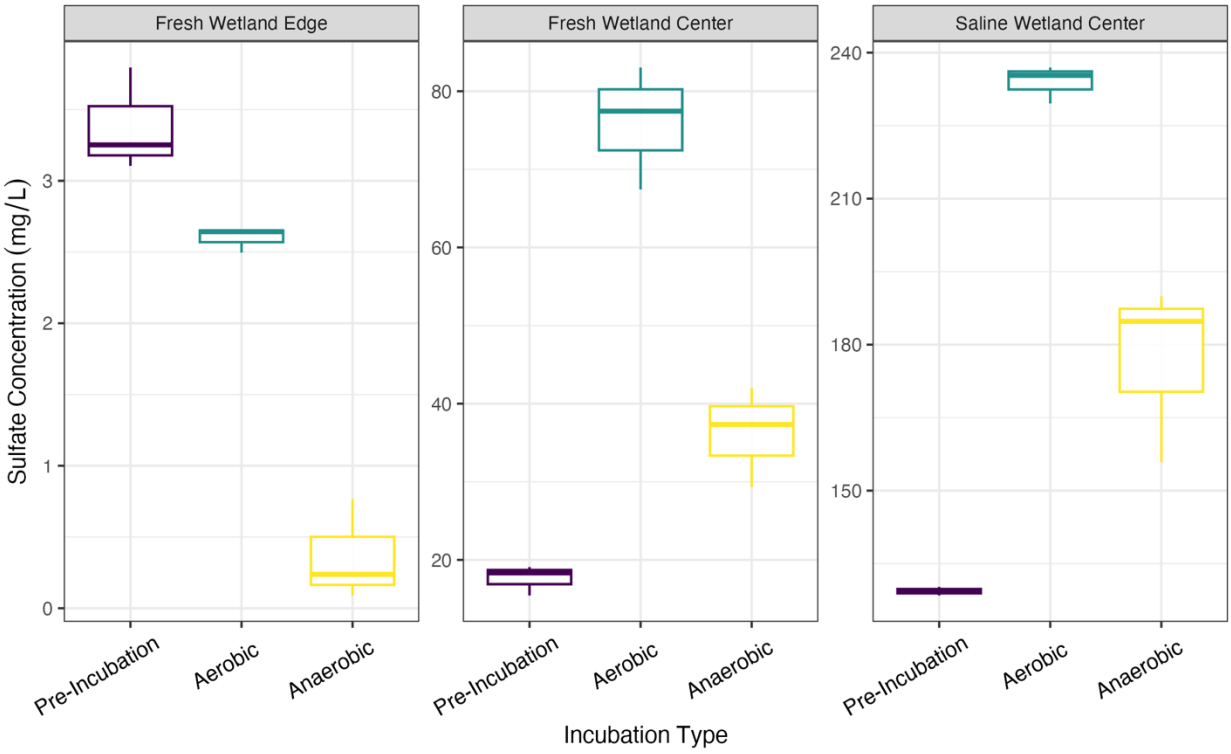

Figure 6. Sulfate concentrations in samples filtered to 0.2 µm pre- and post-incubation. The instrumentation used to measure sulfate did not allow us to analyze by colloidal size fraction without compromising the instrument.

For the SW-C soils, sulfate levels significantly increased ($p < 0.05$) after the 21-day incubation under both aerobic (234 ± 4 mg/L) and anaerobic conditions (177 ± 18 mg/L), indicating that sulfate was not depleted as a terminal electron acceptor despite active sulfate reduction (as suggested by the H_2S scent). Interestingly, sulfate levels also increased ($p < 0.05$) for the FW-C soils under both aerobic (76.0 ± 7.9 mg/L) and anaerobic conditions (36.2 ± 6.4 mg/L), again highlighting the presence of a competing terminal electron acceptor that can inhibit methanogenesis. Though in this case we did not detect an obvious presence of H_2S. It is possible that for FW-C, iron reduction was the dominant constraint on methanogenesis.

Both SW-C and FW-C anaerobic incubations ended with lower sulfate concentrations than their aerobic counterparts (57.1 mg/L and 39.7 mg/L lower for SW-C and FW-C soils, respectively), suggesting a solid phase source of sulfate. Corroborating this result, we also observed a decrease in solid phase sulfur content for the SW-C and FW-C soils under both incubation conditions, except for the FW-C anaerobic incubation (Figure S4). FW-E on the other hand had lower ($p < 0.05$) sulfate concentrations at the end of the incubation under aerobic (2.60 ± 0.09 mg/L) and anaerobic (0.36 ± 0.36 mg/L) conditions, suggesting that sulfur cycling did not play a major role in limiting methane production in this case.

3.4 Organic Carbon Content and Composition

The concentration, size fractionation, and composition of organic carbon was also measured to evaluate if carbon quality could potentially explain differences in GHG production across the different soil types and incubation conditions. Prior to the incubations, the TOC concentration (all size fractions combined) was significantly higher for the SW-C soils (83.0 ± 24.0 mg/L) compared to FW-E (4.97 ± 0.82 mg/L) and FW-C soils (2.59 ± 0.63 mg/L; $p < 0.05$; Figure 7) despite the FW-E solid soils having a higher percent carbon content (Figure S3). Prior to the incubations, TOC in the freshwater samples was dominated by the smallest NP+S size fraction with 64 ± 28% and 70 ± 10% of the aqueous TOC pool present as nanoparticles and soluble carbon for FW-C and FW-E, respectively (Figure 7). In contrast, only 23 ± 9% of the TOC was in the NP+S size fraction for the saline SW-C soils and most of the TOC (58 ± 9%) was in the largest particulate phase prior to incubation. Fine colloids were the smallest part of the aqueous TOC pool, representing 1 ± 2%, 12 ± 11%, and 19 ± 7% of TOC for FW-C, FW-E, and SW-C samples, respectively.

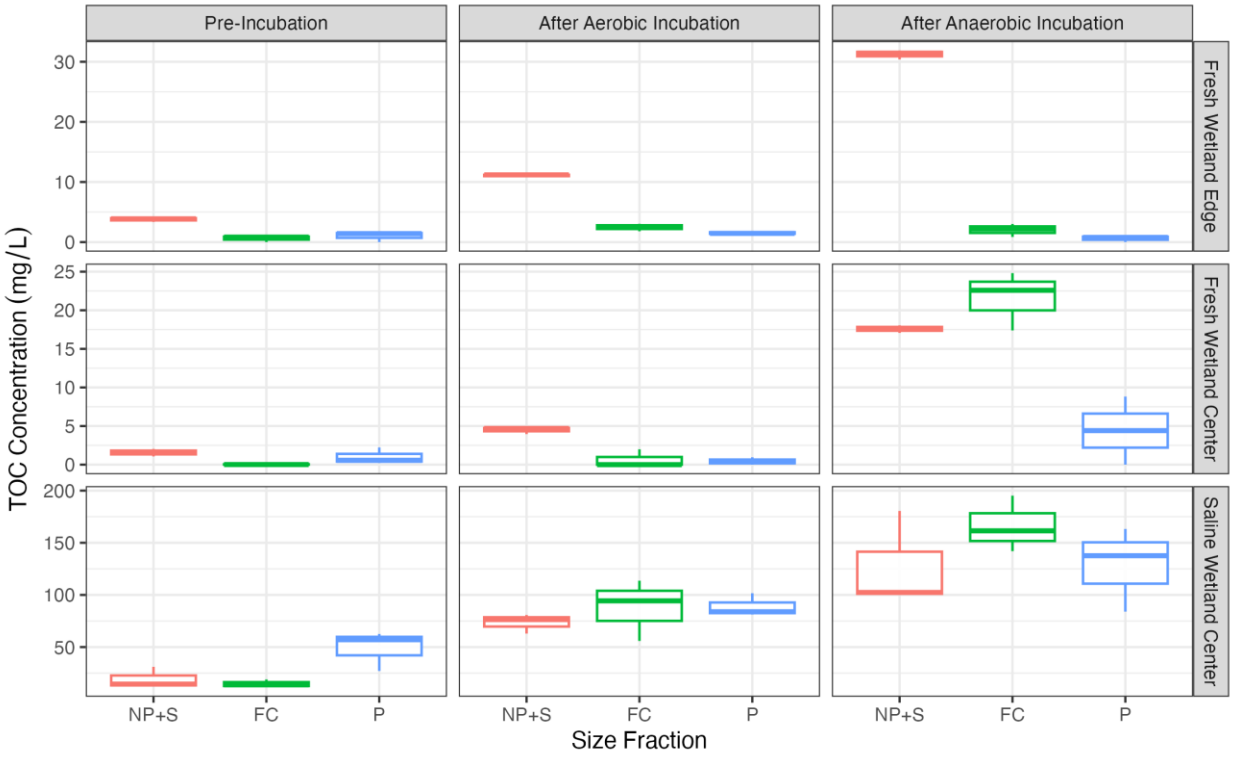

Figure 7. Total organic carbon across size fractions and incubation conditions. The smallest size fraction is nanoparticulates plus truly soluble material (NP+S; <0.1μm), followed by fine colloids (FC; 0.1-0.45μm), then particulates (P; 0.45-1μm).

TOC concentrations increased on average for all size fractions, under both incubation conditions, and across all sites ($p < 0.05$). Across all sites, there was an average 2.8 and 1.8 times increase in particulate TOC, 12.3 and 5.9 times increase in fine colloidal TOC, and 7.2 and 3.6 times increase in nanoparticulate and soluble TOC under anaerobic and aerobic conditions, respectively. Thus, during the incubations, there was a seemingly ample and renewing supply of

carbon to microbial communities with a shift towards a greater proportion of FC and NP+S TOC size fractions; this increase was most evident for the freshwater and saline wetland center sites. At the end of the incubations, the fine colloidal fraction represented 44 ± 8% and 10 ± 17% of the TOC pool for FW-C, 6 ± 3% and 16 ± 4% of the TOC pool for FW-E, and 39 ± 5% and 34 ± 6% of the TOC pool for SW-C soils under anerobic and aerobic conditions, respectively. The nanoparticulate and soluble fraction represented 37 ± 12% and 82 ± 11% of the TOC pool for FW-C, 92 ± 2% and 73 ± 2% of the TOC pool for FW-E, and 30 ± 12% and 30 ± 2% of the TOC pool for SW-C soils under anerobic and aerobic conditions, respectively. Finally, the SW-C soils had substantially higher TOC concentrations compared to the other two soils under both anaerobic and aerobic conditions (Figure 7; $p < 0.05$).

The ratio of TOC to total dissolved nitrogen (C:N ratio) was calculated to assess potential differences in organic matter composition across size fractions (Figure 8). For the saline soils, there was no significant difference in C:N ratios across all size fractions in the pre-incubated samples ($p < 0.05$). The average C:N ratios for all size fractions combined was 11.2 ± 0.5 prior to incubation, 11.2 ± 1.3 under aerobic conditions and 10.2 ± 1.0 under anerobic conditions for SW-C soils.

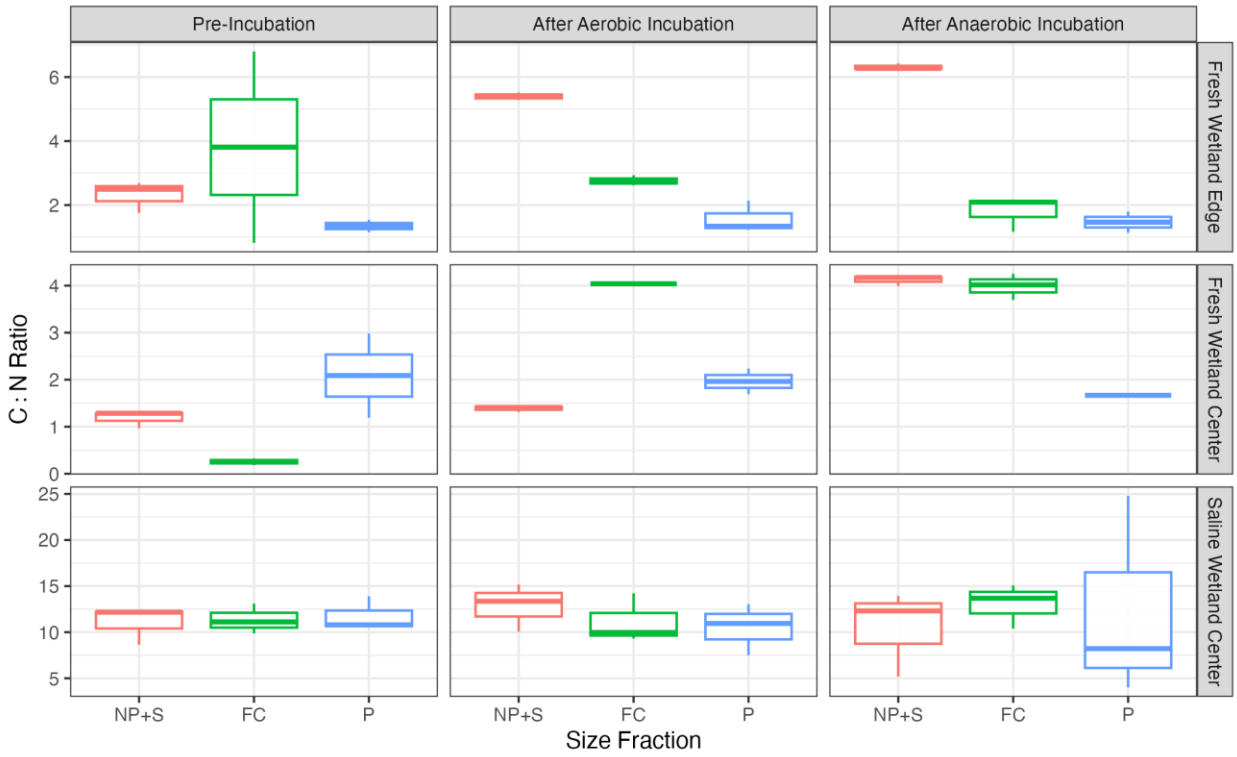

Figure 8. The ratio of total organic carbon to total dissolved nitrogen (C:N) across size fractions and incubation conditions. The smallest size fraction is nanoparticulates plus truly soluble material (NP+S; <0.1µm), followed by fine colloids (FC; 0.1-0.45µm), then particulates (P; 0.45-1µm).

C:N ratios became more variable across the different size fractions under anerobic conditions with average C:N ratios of 12.3 ± 11.0, 13.0 ± 2.4, and 10.5 ± 4.7 for the P, FC, and NP+S size fractions, respectively for SW-C soils (Figure 8), but differences between size fractions were insignificant ($p > 0.05$).

Both freshwater soils had significantly lower C:N ratios than the saline soils, with a pre-incubation average of 1.7 ± 0.2 and 2.1 ± 1.3 for FW-E and FW-C, respectively, when considering all size fractions. For the FW-E soils, average C:N ratios (average of all size fractions) increased significantly under both aerobic (3.8 ± 0.3) and anaerobic (5.3 ± 0.2) conditions ($p < 0.05$). This change in composition was primarily driven by an increase in C:N in the smallest NP+S size fraction (Figure 8), which increased to 5.4 ± 0.1 and 6.3 ± 0.1 under aerobic and anaerobic conditions, respectively ($p < 0.05$). The particulate fraction remained unchanged after the incubations for FW-E soils and there was a slight but insignificant decrease in C:N for the fine colloid fraction ($p > 0.05$). In contrast, FW-C soils only saw an increase in C:N under anerobic conditions when considering all size fractions (3.4 ± 0.8; $p < 0.05$). Similar to FW-E, there was an increase in C:N of the NP+S size fraction under anaerobic conditions (4.1 ± 0.1; $p < 0.05$). C:N for the fine colloid fraction also increased under both incubation conditions for FW-C soils (Figure 8), but it was not possible to perform a statistical analysis due to several samples having carbon and/or nitrogen concentrations of zero. In the solid soil phase, C:N ratios decreased under both incubation conditions for SW-C, increased under both incubation conditions for FW-C, and increased under aerobic conditions but decreased under aerobic conditions for FW-E (Figure S5).

To further examine how carbon quality might have impacted GHG production we analyzed each aqueous TOC size fraction via FT-ICR-MS and estimated the proportion of TOC present in different compound classes. We did not detect significant differences between any of the size fractions (Tables S1-3), so we focus our discussion on a summary of the average composition across all size fractions (Table 1). The lack of variability across size fractions is likely because all samples needed to be subjected to solid phase extraction to prepare samples for analysis; the extraction process likely biases the results towards the composition of soluble TOC. For both freshwater soils, there was a slight increase in the number of unique features (i.e., number of peaks) after being incubated in aerobic conditions, but this change was not significant ($p > 0.05$). In contrast there was a significant decrease in features in the saline soil under both incubation conditions (Table 1; $p < 0.05$) demonstrating a loss of diversity for saline soils.

Table 1. Summary of the total number of peaks detected via FT-ICR-MS and the calculated percent contribution of different compound classes to the portion of the TOC pool captured within the analytical window. The average of all size fractions is presented here, and a breakdown by size fraction can be found in Tables S1-3.

Soil/Incubation Type	FW-E Pre-Incubation	FW-E Aerobic Incubation	FW-E Anaerobic Incubation	FW-C Pre-Incubation	FW-C Aerobic Incubation	FW-C Anaerobic Incubation	SW-C Pre-Incubation	SW-C Aerobic Incubation	SW-C Anaerobic Incubation
Compound Class									
Amino Sugars	5 ± 1	3 ± 0	2 ± 0	5 ± 1	3 ± 1	2 ± 1	4 ± 1	4 ± 1	4 ± 1
Carbohydrates	4 ± 2	2 ± 0	1 ± 1	3 ± 2	2 ± 1	1 ± 0	3 ± 1	2 ± 0	2 ± 0
Condensed Hydrocarbons	12 ± 5	18 ± 4	22 ± 3	14 ± 4	19 ± 3	22 ± 3	14 ± 6	12 ± 5	13 ± 5
Lignin	38 ± 3	50 ± 5	45 ± 1	39 ± 4	48 ± 2	45 ± 2	40 ± 4	35 ± 4	32 ± 4
Lipids	9 ± 3	4 ± 1	6 ± 2	8 ± 3	4 ± 1	6 ± 2	9 ± 5	15 ± 5	17 ± 5
Other	1 ± 0	0 ± 0	0 ± 0	1 ± 0	0 ± 0	0 ± 0	1 ± 0	0 ± 0	0 ± 0
Proteins	22 ± 5	12 ± 1	11 ± 3	21 ± 6	11 ± 2	11 ± 3	17 ± 5	21 ± 5	22 ± 4
Tannins	7 ± 3	10 ± 2	12 ± 2	8 ± 3	11 ± 2	12 ± 2	10 ± 3	8 ± 2	8 ± 2
Unsaturated Hydrocarbons	1 ± 1	1 ± 0	0 ± 0	1 ± 1	1 ± 0	1 ± 0	1 ± 1	2 ± 1	2 ± 1
Number of Peaks	9,888 ± 2,076	10,540 ± 1,673	8,773 ± 1,572	9,706 ± 2,136	10,390 ± 2,432	8,802 ± 1,513	9,688 ± 754	7,976 ± 911	7,243 ± 862

Lignin-like molecules were the dominant compound class for all soils both pre- and post-incubation under both conditions, contributing from 29-49% of the aqueous TOC pool. The proportion of lignin-like TOC in the saline soils significantly decreased under both incubation conditions in contrast to an increase in the proportion of lignin-like TOC for both freshwater soils under both incubation conditions (Table 1; $p < 0.05$). Protein-like molecules were the second most abundant compound class, and similarly had divergent behavior between freshwater and saline soils. In contrast to lignin-like molecules, the proportional abundance of protein-like molecules decreased for both freshwater soils and increased in the saline soils following both incubation conditions ($p < 0.05$). The third most abundant compound classes were lipid-like and condensed hydrocarbon molecules. Condensed hydrocarbons increased in proportional abundance following both incubation conditions in the freshwater soils ($p < 0.05$) but did not change substantially in the saline soils. The relatively labile amino sugar-like TOC fraction only made up ~5% of the TOC pool prior to incubation for all soils but decreased significantly for both freshwater soils under both incubation conditions ($p < 0.05$) but remained unchanged in the incubated saline soils ($p > 0.05$). Carbohydrate-like TOC was similarly abundant prior to incubation and decreased in all soils under all incubation conditions ($p < 0.05$). Tannin-like TOC followed a similar trend, decreasing for all soils under all incubation conditions ($p < 0.05$). Unsaturated hydrocarbons made up a minimal fraction of the TOC pool (i.e., 0-3%) across the soil types and incubation conditions (Table 1).

To compare molecular level data with bulk analyses, we also computed C:N ratios derived from FT-ICR-MS data. Interestingly, the C:N ratios calculated with FT-ICR-MS data were significantly higher ($p < 0.05$) compared to bulk C:N ratios with pre-incubation averages of 30.5 $\pm$ 4.0, 32.0 $\pm$ 5.2, and 31.9 $\pm$ 1.7 for FW-E, FW-C, and SW-C soils, respectively. FT-ICR-MS-derived C:N ratios significantly decreased ($p < 0.05$) for FW-C soils under aerobic conditions (28.8 $\pm$ 2.7) and increased ($p < 0.05$) for SW-C soils under both aerobic (36.4 $\pm$ 3.8) and anaerobic conditions (40.0 $\pm$ 4.5), which in both cases contrasts the trends observed in bulk C:N ratios. These differences between molecular level and bulk characterizations highlight the fact that extracting samples and analyzing via mass spectrometry substantially narrows the analytical window and range of molecules considered for calculations such as C:N ratios.

4 Discussion

4.1 Physiochemical Conditions of the Incubations

The increase in ORP after aerobic (oxidizing) incubation and a decrease in anaerobic (reducing) conditions observed in both freshwater soils was expected (Figure S1). However, the counter-intuitive decrease in ORP in the saline soil even under aerobic conditions may be related to the association of increased ionic concentrations in saline soils with decreased oxygen solubility, which leads to lower redox potentials (Herbert et al. 2015). Porewater dissolved oxygen at the time of soil collection was only 2.2 mg/L at the saline site and all soils were conditioned in an anaerobic chamber for 4 days prior to incubation, so the introduction of oxygen was predicted to increase ORP due to the high redox potential of oxygenated water as a redox pair (Liu et al. 2013). Additionally, anaerobic saline soil incubations were the only ones to reach negative ORP values. The increase in alkalinity and pH after anaerobic incubation of soil-water solutions is also consistent with previous incubation studies (Thompson et al. 2006a, Afsar et al. 2020).

Increases in pH in soils subjected to anoxia have been attributed to dissolution of metal oxyhydroxides and oxides (Dassonville & Renault 2002, Ponnamperuma 1972) and to consumption of H^+ in Fe-oxide reduction (Thompson et al. 2006b, Lindsay 1979). Alkalinity increased to the greatest degree in saline soils in which sulfate reduction likely occurred, a reaction type that yields bicarbonate (Van Breemen 1987).

4.2 Organic Carbon Content and Composition

Substantial amounts of both carbon and nitrogen were released from the soil over the course of the incubations (Figures 7-8), implying that the rate of release exceeded the rate of biodegradation. As in prior studies (e.g., Reddy & Patrick 1975, Yan et al. 2016, Bhattacharyya et al. 2018), TOC concentrations at the end of the incubation were far greater under anaerobic conditions compared to aerobic (Figure 7). Anaerobic water saturated soils tend to exhibit higher concentrations of organic matter *in situ* than aerobic soils due to multiple physical, chemical, and metabolic factors (Marschner 2021). Based on the differences we observed between the same soils exposed to aerobic or anaerobic conditions, some potential mechanisms limiting carbon biodegradation and promoting carbon accumulation in these experiments may be the low energetic efficiency of anaerobic decomposition (Ponneperuma 1972) and anoxic constraint of phenol oxidase enzymes (Dunn & Freeman 2018).

Final concentrations of TOC in the saline soil incubates were an order of magnitude higher than in freshwater soils, which is interesting given that salinity is associated with increased activity of carbon-degrading enzymes (Morrissey et al. 2014) and thus could be expected to have increased biodegradation. Likewise, soil extractions with seawater tend to yield lower DOC release, potentially attributable in part due to flocculation of OM in response to higher ionic strength (Dou et al. 2008, Kida et al. 2017). However, in the case of our incubations, the saline soils were exposed to freshwater. Decreasing the ionic strength of soil-water solutions can expand the diffuse double layer, causing disaggregation and destabilization of associations between OM and minerals and an increase in released TOC (Kleber et al. 2021; Tomaszewski et al. 2021).

Iron cycling is another factor that may have influenced the amount and size of TOC released for the different soils under anerobic conditions. Mineral iron oxides bound to OM can be reduced under anoxic conditions, releasing the OM formerly bound in soil (Zhao et al. 2017, Grybos et al. 2009). Indeed, we observed an increase in both NP+S, fine colloidal, and particulate TOC for both the SW-C and FW-C soils, which had high levels of reduced Fe^{2+}, whereas the FW-E soil showed no evidence of iron reduction and did not release mineral-associated fine colloidal or particulate TOC (Figures 5 and 7). The majority of OC of the size fractions examined was present in the nanoparticulate and truly soluble fraction in freshwater soils, which follows the trend seen by Afsar et al. (2020) in experiments with another freshwater wetland soil. Their observation of OC in nanoparticulate size fractions being more redox-dependent than in particulate size fractions also agrees with the higher increases in TOC concentrations observed here in the smallest size fraction. Two exceptions to this trend were anaerobic incubations of freshwater and saline wetland center soils; these soils also showed low CO_2 and methane production compared to aerobic samples.

One other factor that may have resulted in the observed differences in TOC size fractions between the freshwater and saline sites is different vegetation characteristics of the sites. The

saline Beaver Creek soils had a high abundance of root biomass and other plant detritus associated with marsh grass (Sengupta et al., 2019), which likely contributed to the high particulate TOC abundance compared to the freshwater soils. Vegetation composition at the freshwater site, Old Woman Creek, on the other hand is more variable over time due to complex flooding and drying regimes; depending on annual water levels, vegetation at the wetland site that was sampled can vary between different macrophytes such as water lily, lotus, or cattail cover (Villa et al., 2020). At the time of sampling, the freshwater wetland sites were not inundated and had minimal live vegetation present.

4.3 Greenhouse Gas Production and Competing Redox Reactions

The low methane production in both fresh and saline wetland center soils can be attributed to the reduction of species (e.g., NO_3^-, MnO_2, Fe^{3+}, SO_4^{2-}) higher on the redox ladder outcompeting methanogenesis. Nitrate was depleted for all soil types under anerobic conditions. Iron reduction was prominent for both wetland center soils as shown by Fe^{2+} concentrations (Figure 5) and was likely an important reaction competing with methanogenesis similar to findings from other experimental studies (e.g., Helton et al. 2019). Interestingly, the FW-E soils, which produced 47 times more methane under anaerobic conditions than the FW-C soils (Figure 2), had higher pre-incubation concentrations of total iron than the FW-C soil (Figure 4). However, FW-E did not produce appreciable amounts of Fe^{2+}, suggesting that significant iron reduction did not occur in the wetland edge soil and/or there was not a prominent solid phase iron source. A variety of factors are known to influence the availability of Fe^{3+} in soils, including acidic pH and low ORP (Colombo et al. 2014). The freshwater wetland center soil, which appeared to host iron reduction, had lower pH values during anaerobic incubations than the wetland edge soil, though not as acidic as conditions typically associated with high iron solubility (Borch 2010). Low redox potential is also associated with iron reduction, and the FW-E soil, which had no increase in Fe^{2+}, did have higher redox potentials than the other soils. Methane production took about four days to initiate in the FW-E soils, perhaps as a result of competing redox reactions that exhausted all available terminal electron acceptors (Figure 2). This difference in iron cycling between the two freshwater sites perhaps related to the fact that FW-C soils are more frequently flooded and anoxic compared to FW-E, which is only periodically inundated (USDA Natural Resources Conservation Service n.d).

Sulfate reduction was another important competing redox reaction in the saline soil under anaerobic conditions. Although we cannot discount sulfate reduction as a competing reaction with methanogenesis for the freshwater wetland center soil, which had high levels of sulfate (Figure 6), the odor of H_2S emerging from the saline samples is clear evidence that sulfate reduction was active for the saline soils. Solid phase sulfur content was relatively high in the saline soil prior to incubations, and decreased markedly under both incubation conditions (Figure S4). Potential sources of sulfate might include oxidation of iron and sulfur containing minerals under aerobic conditions or reductive dissolution of minerals under anaerobic conditions (Van Breemen 1988). It is unclear how long the soils would need to be incubated (or flooded in the case of the natural ecosystem setting) to exhaust the large source of mineral sulfur and initiate methanogenesis, particularly for the saline soil.

Experimental results from this study highlight the importance in considering the diversity of size fractions present in soil-water matrices for interpreting drivers of GHG production. For example,

results from the anaerobic incubation showed that iron reduction played a direct role in limiting methane production. However, measuring dissolved iron via filtration would have masked this finding. The majority of Fe^{2+} in soils with high concentrations was measured in the largest particulate size fraction (0.45 – 1 μm). Colloids greater than 0.45 μm are often excluded from studies of OM characterization and/or GHG production, but in this study the larger size fraction was key in providing evidence for iron reduction as a competing redox reaction and potential mechanism for mineral-associated TOC release.

Considering colloidal and particulate size fractions of TOC also yielded insight into the mechanisms underlying different responses in aerobic CO_2 production across the different soil types. Aerobic CO_2 production was highest for both freshwater soils, which had a much higher proportion of pre-incubation OM in the NP+S fraction (64 ± 28% and 70 ± 10% for FW-C and FW-E, respectively) compared to the SW-C soil (24 ± 9%). This finding contrasts conceptual models for OM bioavailability in aquatic settings. For example, larger colloidal and particulate OM is thought to be more bioavailable in marine surface waters (Benner and Amon, 2015), but active association or disassociation with mineral surfaces may complicate this model in terrestrial systems (Yan et al. 2018).

TOC quantity was clearly not the primary driver of aerobic respiration in our experiments considering the low CO_2 production for SW-C soils (Figure 1), which had an order of magnitude higher TOC content (Figure 7). Rather, carbon quality was likely a key constraint on aerobic respiration. The freshwater soils not only had a higher proportion of truly soluble and nanoparticulate TOC that remained unassociated with minerals, they also had a substantially higher amount of nitrogen relative to carbon compared to the SW-C soils. The very low C:N ratios in the freshwater soils (1.7 ± 0.2 and 1.4 ± 0.3 for FW-E and FW-C, respectively) are reflective of microbial detritus, whereas the C:N ratios for SW-C of 11.2 ± 0.5 are more reflective of vegetation detritus (Bianchi et al. 2007). This microbially-derived OM appeared to be much more readily bioavailable compared to the OM present in the SW-C soils, which is consistent with observations that low C:N ratios in soils is often highly bioavailable (Liu et al. 2016). These differences in OM composition would not have been as evident without examining the elemental composition of different size fractions. Our characterization of OM composition via FT-ICR-MS, alone, would have suggested a more homogenous composition across soils and incubations (Table 1) due to the smaller analytical window this method provides (Qi et al. 2022).

5 Conclusions

Coastal wetlands contain dynamic carbon pools that are anticipated to face increased stressors in the form of SLR and increased occurrence and severity of extreme weather events (Ward et al. 2020, LaFond-Hudson and Sulman, 2023). These changes are expected to alter coastal wetland redox conditions (Regier et al. 2023) and organic matter cycling (Smith et al. 2023). In this study, we experimentally probed several major gaps in our understanding of the properties and processes that mediate 1) GHG emissions from coastal wetlands and 2) the mobility of carbon in coastal wetland soils across a more complete size class spectrum than is typically studied.

First, we quantified how the presence of a variety of terminal electron acceptors (i.e., nitrate, iron, and sulfate) associated with distinct soil types and inundation history inhibit methane production under anaerobic conditions. By characterizing a spectrum of different size fractions

(e.g., soluble, nanoparticulates, fine colloids, and particulates), we were able to develop mechanistic insight into why and under what conditions certain redox reactions can limit methanogenesis. We found that reduction of mineral-phase iron into particulate and colloidal Fe^{2+} was one major factor limiting methanogenesis in both fresh and saline wetland center soils along with sulfate reduction in the saline soil.

We used the same size fractionation technique to characterize the aqueous organic matter pool to mechanistically understand why aerobic CO_2 production varied substantially across the three different studied soils. We found that soils with a higher proportion of soluble molecules had substantially higher rates of aerobic respiration compared to soils with a higher proportion of colloidal and particulate carbon. Likewise, we found that carbon quality was more important than carbon quantity in driving high respiration rates. Finally, we found that colloidal organic matter could be a prominent, and overlooked, component of the pool of carbon that is mobile in wetland soil environments, particularly for the saline soils we investigated. The high proportion of colloidal OM found in the saline wetland soil, OM that typically goes uncharacterized, may be a major component of the carbon that is laterally transported from coastal wetlands to the ocean.

Acknowledgments

This research was performed on project award 60097 from the Environmental Molecular Sciences Laboratory, a DOE Office of Science User Facility sponsored by the Biological and Environmental Research program under Contract No. DE-AC05-76RL01830. The samples used for this study were collected at field sites stewarded by COMPASS-FME, a multi-institutional project supported by DOE-BER as part of the Environmental System Science Program. We thank the University of Toledo field team for support maintaining the research sites and Kaizad Patel for helping with soil sample collection at Old Woman Creek. We thank Don Lentz, the Hancock Timber Company, and Washington Department of Fish & Wildlife for access to the Beaver Creek field site. We thank the NOAA-NERR program for access to the Old Woman Creek site and producing the datasets used for site context. Data were collected via the NERR System-wide Monitoring Program (https://cdmo.baruch.sc.edu/) for Old Woman Creek. We thank Kathleen Munson and Nubia Nieto Pereira for assistance with ICP-OES analyses as well as Opal Otenburg and Allison Myers-Pigg for ion chromatograph analyses.

Open Research

All data used in this study are available at the Figshare.com repository via https://doi.org/10.6084/m9.figshare.c.6827016.v3 with a publicly available CC BY 4.0 license. To elevate findability by the biogeosciences community, the final dataset will be cross-referenced on the Environmental System Science Data Infrastructure for a Virtual Ecosystem (ESS-DIVE) data repository upon acceptance of the manuscript.

References

Afsar, M. Z., Goodwin, C., Beebe Jr, T. P., Jaisi, D. P., & Jin, Y. (2020). Quantification and molecular characterization of organo-mineral associations as influenced by redox oscillations. Science of the Total Environment, 704, 135454.

Afsar, M.Z., Vasilas, B. & Jin, Y. (2023). Organo-mineral associations and size-fractionated colloidal organic carbon dynamics in a redox-controlled wetland. Geoderma, 439, 116667.

Altor, A. E., & Mitsch, W. J. (2008). Pulsing hydrology, methane emissions and carbon dioxide fluxes in created marshes: A 2-year ecosystem study. Wetlands, 28(2), 423-438.

Bailey, V. L., Smith, A. P., Tfaily, M., Fansler, S. J., & Bond-Lamberty, B. (2017). Differences in soluble organic carbon chemistry in pore waters sampled from different pore size domains. Soil Biology and Biochemistry, 107, 133-143.

Benner, R., & Amon, R. M. (2015). The size-reactivity continuum of major bioelements in the ocean. Annual review of marine science, *7*, 185-205.

Bhattacharyya, A., Campbell, A. N., Tfaily, M. M., Lin, Y., Kukkadapu, R. K., Silver, W. L., ... & Pett-Ridge, J. (2018). Redox fluctuations control the coupled cycling of iron and carbon in tropical forest soils. Environmental science & technology, 52(24), 14129-14139.

Bianchi, T. S., Wysocki, L. A., Stewart, M., Filley, T. R., & McKee, B. A. (2007). Temporal variability in terrestrially-derived sources of particulate organic carbon in the lower Mississippi River and its upper tributaries. Geochimica et Cosmochimica Acta, *71*(18), 4425-4437.

Borch, T., Kretzschmar, R., Kappler, A., Cappellen, P. V., Ginder-Vogel, M., Voegelin, A., & Campbell, K. (2010). Biogeochemical redox processes and their impact on contaminant dynamics. Environmental science & technology, 44(1), 15-23.

Buettner, S. W., Kramer, M. G., Chadwick, O. A., & Thompson, A. (2014). Mobilization of colloidal carbon during iron reduction in basaltic soils. Geoderma, 221, 139-145.

Chen, C., Hall, S. J., Coward, E., & Thompson, A. (2020). Iron-mediated organic matter decomposition in humid soils can counteract protection. Nature communications, 11(1), 1-13.

Chu, S. N., Wang, Z. A., Gonneea, M. E., Kroeger, K. D., & Ganju, N. K. (2018). Deciphering the dynamics of inorganic carbon export from intertidal salt marshes using high-frequency measurements. Marine Chemistry, *206*, 7-18.

Clark, J. M., Lane, S. N., Chapman, P. J., & Adamson, J. K. (2007). Export of dissolved organic carbon from an upland peatland during storm events: Implications for flux estimates. Journal of Hydrology, 347(3-4), 438-447.

Colombo, C., Palumbo, G., He, J. Z., Pinton, R., & Cesco, S. (2014). Review on iron availability in soil: interaction of Fe minerals, plants, and microbes. Journal of soils and sediments, 14(3), 538-548.

Dassonville, F., & Renault, P. (2002). Interactions between microbial processes and geochemical transformations under anaerobic conditions: a review. Agronomie, 22(1), 51-68.

Dittmar, T., Koch, B., Hertkorn, N., &; Kattner, G. (2008). A simple and efficient method for The Solid-phase extraction of dissolved organic matter (SPE-DOM) from seawater. Limnology and Oceanography: Methods, 6(6), 230-235. doi:10.4319/lom.2008.6.230

Dou, F., Ping, C. L., Guo, L., & Jorgenson, T. (2008). Estimating the impact of seawater on the production of soil water-extractable organic carbon during coastal erosion. Journal of environmental quality, 37(6), 2368-2374.

Dunn, C., & Freeman, C. (2018). The role of molecular weight in the enzyme-inhibiting effect of phenolics: the significance in peatland carbon sequestration. Ecological Engineering, 114, 162-166.

759 Feng, J., & Hsieh, Y. P. (1998). Sulfate reduction in freshwater wetland soils and the effects of
760 sulfate and substrate loading (Vol. 27, No. 4, pp. 968-972). American Society of
761 Agronomy, Crop Science Society of America, and Soil Science Society of America.
762 Freeman, C., Ostle, N., & Kang, H. (2001). An enzymic 'latch' on a global carbon store. Nature,
763 409(6817), 149-149.
764 Grybos, M., Davranche, M., Gruau, G., Petitjean, P., & Pédrot, M. (2009). Increasing pH drives
765 organic matter solubilization from wetland soils under reducing conditions. Geoderma,
766 154(1-2), 13-19.
767 Helton, A. M., Ardón, M., & Bernhardt, E. S. (2019). Hydrologic context alters greenhouse gas
768 feedbacks of coastal wetland salinization. Ecosystems, 22(5), 1108-1125.mm
769 Herbert, E. R., Boon, P., Burgin, A. J., Neubauer, S. C., Franklin, R. B., Ardón, M., ... & Gell, P.
770 (2015). A global perspective on wetland salinization: ecological consequences of a
771 growing threat to freshwater wetlands. Ecosphere, 6(10), 1-43.
772 Ho, D. T., Ferrón, S., Engel, V. C., Anderson, W. T., Swart, P. K., Price, R. M., & Barbero, L.
773 (2017). Dissolved carbon biogeochemistry and export in mangrove-dominated rivers of
774 the Florida Everglades. *Biogeosciences*, *14*(9), 2543-2559.
775 Kida, M., Tomotsune, M., Iimura, Y., Kinjo, K., Ohtsuka, T., & Fujitake, N. (2017). High
776 salinity leads to accumulation of soil organic carbon in mangrove soil. Chemosphere, 177,
777 51-55.
778 Kim, H. S., & Pfaender, F. K. (2005). Effects of microbially mediated redox conditions on
779 PAH− soil interactions. Environmental science & technology, 39(23), 9189-9196.
780 Kleber, M., Bourg, I. C., Coward, E. K., Hansel, C. M., Myneni, S. C., & Nunan, N. (2021).
781 Dynamic interactions at the mineral–organic matter interface. Nature Reviews Earth &
782 Environment, *2*(6), 402-421.
783 Lal, R., Monger, C., Nave, L., & Smith, P. (2021). The role of soil in regulation of climate.
784 Philosophical Transactions of the Royal Society B, 376(1834), 20210084.
785 LaFond-Hudson, S., & Sulman, B. (2023). Modeling strategies and data needs for representing
786 coastal wetland vegetation in land surface models. New Phytologist, 238(3), 938-951.
787 Lindsay, W. L. (1979). Chemical equilibria in soils. John Wiley and Sons Ltd..
788 Liu, C. G., Xue, C., Lin, Y. H., & Bai, F. W. (2013). Redox potential control and applications in
789 microaerobic and anaerobic fermentations. Biotechnology advances, 31(2), 257-265.
790 Liu, M., Ussiri, D. A., & Lal, R. (2016). Soil organic carbon and nitrogen fractions under
791 different land uses and tillage practices. Communications in Soil Science and Plant
792 Analysis, 47(12), 1528-1541.
793 Lønborg, C., Carreira, C., Jickells, T., & Álvarez-Salgado, X. A. (2020). Impacts of global
794 change on ocean dissolved organic carbon (DOC) cycling. Frontiers in Marine Science, 7,
795 466.
796 Magen, C., Lapham, L. L., Pohlman, J. W., Marshall, K., Bosman, S., Casso, M., & Chanton, J.
797 P. (2014). A simple headspace equilibration method for measuring dissolved methane.
798 Limnology and Oceanography: Methods, 12(9), 637-650.
799 Maher, D.T., Santos, I.R., Golsby-Smith, L., Gleeson, J. and Eyre, B.D., 2013. Groundwater-
800 derived dissolved inorganic and organic carbon exports from a mangrove tidal creek: The
801 missing mangrove carbon sink?. Limnology and Oceanography, 58(2), pp.475-488.
802 Marín-Spiotta, E., Gruley, K. E., Crawford, J., Atkinson, E. E., Miesel, J. R., Greene, S., ... &
803 Spencer, R. G. M. (2014). Paradigm shifts in soil organic matter research affect

interpretations of aquatic carbon cycling: transcending disciplinary and ecosystem boundaries. Biogeochemistry, 117(2), 279-297.

Marschner, P. (2021). Processes in submerged soils–linking redox potential, soil organic matter turnover and plants to nutrient cycling. Plant and Soil, 464(1), 1-12.

Moomaw, W. R., Chmura, G. L., Davies, G. T., Finlayson, C. M., Middleton, B. A., Natali, S. M., ... & Sutton-Grier, A. E. (2018). Wetlands in a changing climate: science, policy and management. Wetlands, 38(2), 183-205.

Morrissey, E. M., Gillespie, J. L., Morina, J. C., & Franklin, R. B. (2014). Salinity affects microbial activity and soil organic matter content in tidal wetlands. Global change biology, 20(4), 1351-1362.

Neubauer, S. C., Franklin, R. B., & Berrier, D. J. (2013). Saltwater intrusion into tidal freshwater marshes alters the biogeochemical processing of organic carbon. Biogeosciences, 10(12), 8171-8183.

NOAA National Estuarine Research Reserve System (NERRS). System-wide Monitoring Program. Data accessed from the NOAA NERRS Centralized Data Management Office website: http://www.nerrsdata.org; accessed 5 October 2022.

Noe, G. B., Krauss, K. W., Lockaby, B. G., Conner, W. H., & Hupp, C. R. (2013). The effect of increasing salinity and forest mortality on soil nitrogen and phosphorus mineralization in tidal freshwater forested wetlands. Biogeochemistry, 114(1), 225-244.

Olsson, L., Ye, S., Yu, X., Wei, M., Krauss, K. W., & Brix, H. (2015). Factors influencing CO2 and CH4 emissions from coastal wetlands in the Liaohe Delta, Northeast China. Biogeosciences, 12(16), 4965-4977.

Orton, D.J., Tfaily, M.M., Moore, R.J., LaMarche, B.L., Zheng, X., Fillmore, T.L., Chu, R.K., Weitz, K.K., Monroe, M.E., Kelly, R.T. and Smith, R.D. (2018). A customizable flow injection system for automated, high throughput, and time sensitive ion mobility spectrometry and mass spectrometry measurements. Analytical chemistry, 90(1), pp.737-744.

Parkin, T. B. (1987). Soil microsites as a source of denitrification variability. Soil Science Society of America Journal, 51(5), 1194-1199.

Patel, K. F., Bond-Lamberty, B., Jian, J., Morris, K. A., McKever, S. A., Norris, C. G., ... & Bailey, V. L. (2022). Carbon flux estimates are sensitive to data source: a comparison of field and lab temperature sensitivity data. Environmental Research Letters, 17(11), 113003.

Poffenbarger, H. J., Needelman, B. A., & Megonigal, J. P. (2011). Salinity influence on methane emissions from tidal marshes. Wetlands, 31(5), 831-842.

Ponnamperuma, F. N. (1972). The chemistry of submerged soils. Advances in agronomy, 24, 29-96.

Qi, Y., Xie, Q., Wang, J. J., He, D., Bao, H., Fu, Q. L., ... & Fu, P. (2022). Deciphering dissolved organic matter by Fourier transform ion cyclotron resonance mass spectrometry (FT-ICR MS): from bulk to fractions and individuals. Carbon Research, *1*(1), 3.

Qu, W., Li, J., Han, G., Wu, H., Song, W., & Zhang, X. (2019). Effect of salinity on the decomposition of soil organic carbon in a tidal wetland. Journal of Soils and Sediments, 19(2), 609-617.

R Core Team. (2021). R: A language and environment for statistical computing. R Foundation for Statistical Computing, Vienna, Austria.

Reddy, K. R., & Patrick Jr, W. H. (1975). Effect of alternate aerobic and anaerobic conditions on redox potential, organic matter decomposition and nitrogen loss in a flooded soil. Soil Biology and Biochemistry, 7(2), 87-94.

Regier, P., Ward, N. D., Indivero, J., Wiese Moore, C., Norwood, M., & Myers-Pigg, A. (2021). Biogeochemical control points of connectivity between a tidal creek and its floodplain. Limnology and Oceanography Letters, 6(3), 134-142.

Regier, P. J., Ward, N. D., Myers-Pigg, A. N., Grate, J., Freeman, M. J., & Ghosh, R. N. (2023). Seasonal drivers of dissolved oxygen across a tidal creek–marsh interface revealed by machine learning. Limnology and Oceanography.

Rod, K. A., Patel, K. F., Kumar, S., Cantando, E., Leng, W., Kukkadapu, R. K., ... & Kemner, K. M. (2020). Dispersible Colloid Facilitated Release of Organic Carbon From Two Contrasting Riparian Sediments. Frontiers in Water, 2, 67.

Rodrigo-Comino, J., López-Vicente, M., Kumar, V., Rodríguez-Seijo, A., Valkó, O., Rojas, C., ... & Panagos, P. (2020). Soil science challenges in a new era: a transdisciplinary overview of relevant topics. Air, Soil and Water Research, 13, 1178622120977491.

Santos, I. R., Burdige, D. J., Jennerjahn, T. C., Bouillon, S., Cabral, A., Serrano, O., ... & Tamborski, J. J. (2021). The renaissance of Odum's outwelling hypothesis in'Blue Carbon'science. Estuarine, Coastal and Shelf Science, 255, 107361.

Schmidt, M. W., Torn, M. S., Abiven, S., Dittmar, T., Guggenberger, G., Janssens, I. A., ... & Trumbore, S. E. (2011). Persistence of soil organic matter as an ecosystem property. Nature, 478(7367), 49-56.

Sengupta, A., Indivero, J., Gunn, C., Tfaily, M.M., Chu, R.K., Toyoda, J., Bailey, V.L., Ward, N.D. and Stegen, J.C. (2019). Spatial gradients in soil-carbon character of a coastal forested floodplain are associated with abiotic features, but not microbial communities. Biogeosciences, 16, 3911-3928.

Sengupta, A., Stegen, J.C., Bond-Lamberty, B., Rivas-Ubach, A., Zheng, J., Handakumbura, P.P., Norris, C., Peterson, M.J., Yabusaki, S.B., Bailey, V.L. and Ward, N.D. (2021). Antecedent conditions determine the biogeochemical response of coastal soils to seawater exposure. Soil Biology and Biochemistry, 153, 108104.

Sjögersten, S., Black, C. R., Evers, S., Hoyos-Santillan, J., Wright, E. L., & Turner, B. L. (2014). Tropical wetlands: a missing link in the global carbon cycle?. Global biogeochemical cycles, 28(12), 1371-1386.

Smith, A. J., McGlathery, K., Chen, Y., Ewers Lewis, C. J., Doney, S. C., Gedan, K., ... & Kirwan, M. L. (2023). Compensatory Mechanisms Absorb Regional Carbon Losses Within a Rapidly Shifting Coastal Mosaic. Ecosystems, 1-15.

Spivak, A. C., Sanderman, J., Bowen, J. L., Canuel, E. A., & Hopkinson, C. S. (2019). Global-change controls on soil-carbon accumulation and loss in coastal vegetated ecosystems. Nature Geoscience, 12(9), 685-692.

Stagg, C. L., Baustian, M. M., Perry, C. L., Carruthers, T. J., & Hall, C. T. (2018). Direct and indirect controls on organic matter decomposition in four coastal wetland communities along a landscape salinity gradient. Journal of Ecology, 106(2), 655-670.

Stagg, C. L., Schoolmaster, D. R., Krauss, K. W., Cormier, N., & Conner, W. H. (2017). Causal mechanisms of soil organic matter decomposition: deconstructing salinity and flooding impacts in coastal wetlands. Ecology, 98(8), 2003-2018.

Stockmann, U., Adams, M. A., Crawford, J. W., Field, D. J., Henakaarchchi, N., Jenkins, M., ... & Zimmermann, M. (2013). The knowns, known unknowns and unknowns of sequestration of soil organic carbon. Agriculture, Ecosystems & Environment, 164, 80-99.

Stookey, L. L. (1970). Ferrozine---a new spectrophotometric reagent for iron. Analytical chemistry, 42(7), 779-781.

Thompson, A., Chadwick, O. A., Boman, S., & Chorover, J. (2006a). Colloid mobilization during soil iron redox oscillations. Environmental science & technology, 40(18), 5743-5749.

Thompson, A., Chadwick, O. A., Rancourt, D. G., & Chorover, J. (2006b). Iron-oxide crystallinity increases during soil redox oscillations. Geochimica et Cosmochimica Acta, 70(7), 1710-1727.

Tolić, N., Liu, Y., Liyu, A., Shen, Y., Tfaily, M.M., Kujawinski, E.B., Longnecker, K., Kuo, L.J., Robinson, E.W., Paša-Tolić, L. and Hess, N.J. (2017). Formularity: software for automated formula assignment of natural and other organic matter from ultrahigh-resolution mass spectra. Analytical chemistry, 89(23), pp.12659-12665.

Tomaszewski, E. J., Coward, E. K., & Sparks, D. L. (2021). Ionic strength and species drive iron–carbon adsorption dynamics: implications for carbon cycling in future coastal environments. *Environmental Science & Technology Letters*, *8*(8), 719-724.

Tully, K., Gedan, K., Epanchin-Niell, R., Strong, A., Bernhardt, E. S., BenDor, T., ... & Weston, N. B. (2019). The invisible flood: The chemistry, ecology, and social implications of coastal saltwater intrusion. BioScience, 69(5), 368-378.

USDA Natural Resources Conservation Service. (n.d.). Web soil survey. Retrieved November 7, 2019 for Beaver Creek and November 22, 2023 for Old Woman Creek, from https://websoilsurvey.nrcs.usda.gov/app/WebSoilSurvey.aspx

Van Breemen, N. (1987). Effects of redox processes on soil acidity. Netherlands Journal of Agricultural Science, 35(3), 271-279.

Van Breemen, N. (1988). Redox processes of iron and sulfur involved in the formation of acid sulfate soils. In *Iron in soils and clay minerals* (pp. 825-841). Dordrecht: Springer Netherlands.

Villa, J. A., & Bernal, B. (2018). Carbon sequestration in wetlands, from science to practice: An overview of the biogeochemical process, measurement methods, and policy framework. Ecological Engineering, 114, 115-128.

Villa, J. A., Ju, Y., Stephen, T., Rey-Sanchez, C., Wrighton, K. C., & Bohrer, G. (2020). Plant-mediated methane transport in emergent and floating-leaved species of a temperate freshwater mineral-soil wetland. Limnology and Oceanography, 65(7), 1635-1650.

Wang, F., Lu, X., Sanders, C. J., & Tang, J. (2019). Tidal wetland resilience to sea level rise increases their carbon sequestration capacity in United States. Nature communications, 10(1), 1-11.

Wang, Y., Wang, H., He, J. S., & Feng, X. (2017). Iron-mediated soil carbon response to water-table decline in an alpine wetland. Nature communications, 8(1), 1-9.

Wanninkhof, R. (2014). Relationship between wind speed and gas exchange over the ocean revisited. Limnology and Oceanography: Methods, 12(6), 351-362.

Ward, N. D., Megonigal, J. P., Bond-Lamberty, B., Bailey, V. L., Butman, D., Canuel, E. A., ... & Windham-Myers, L. (2020). Representing the function and sensitivity of coastal interfaces in Earth system models. Nature Communications, 11(1), 1-14.

Wiesenburg, D. A., & Guinasso Jr, N. L. (1979). Equilibrium solubilities of methane, carbon monoxide, and hydrogen in water and sea water. Journal of chemical and engineering data, 24(4), 356-360.

Weiss, R. F., & Price, B. A. (1980). Nitrous oxide solubility in water and seawater. Marine chemistry, 8(4), 347-359.

Weston, N. B., Vile, M. A., Neubauer, S. C., & Velinsky, D. J. (2011). Accelerated microbial organic matter mineralization following salt-water intrusion into tidal freshwater marsh soils. Biogeochemistry, 102(1), 135-151.

Wuebbles, D., Cardinale, B., Cherkauer, K., Davidson-Arnott, R., Hellmann, J., Infante, D. and Ballinger, A. (2019). An assessment of the impacts of climate change on the Great Lakes. Environmental Law & Policy Center, 760.

Yabusaki, S. B., Myers-Pigg, A. N., Ward, N. D., Waichler, S. R., Sengupta, A., Hou, Z., ... & Gunn, C. M. (2020). Floodplain inundation and salinization from a recently restored first-order tidal stream. Water Resources Research, 56(7), e2019WR026850.

Yan, J., Lazouskaya, V., & Jin, Y. (2016). Soil colloid release affected by dissolved organic matter and redox conditions. Vadose Zone Journal, 15(3).

Yan, J., Manelski, R., Vasilas, B., & Jin, Y. (2018). Mobile colloidal organic carbon: an underestimated carbon pool in global carbon cycles?. Frontiers in Environmental Science, 6, 148.

Yu, C., Xie, S., Song, Z., Xia, S., & Åström, M. E. (2021). Biogeochemical cycling of iron (hydr-) oxides and its impact on organic carbon turnover in coastal wetlands: A global synthesis and perspective. Earth-Science Reviews, 218, 103658.

Zhang, J., Wang, J. J., Xiao, R., Deng, H., & DeLaune, R. D. (2022). Effect of salinity on greenhouse gas production and emission in marsh soils during the decomposition of wetland plants. Journal of Soils and Sediments, 1-14.